ChemComm

ROYAL SOCIETY OF CHEMISTRY

COMMUNICATION

View Article Online
View Journal | View Issue

Cite this: *Chem. Commun.*, 2023, 59, 896

Received 30th November 2022,
Accepted 13th December 2022

DOI: 10.1039/d2cc06512f

rsc.li/chemcomm

Reversible dynamic optical sensing based on coumarin modified β-cyclodextrin for glutathione in living cells†

Zhixue Liu,[a] Mengdi Tian,[c] Heng Zhang[c] and Yu Liu *[ab]

Coumarin acting as an optical probe was modified on ethylenediamine β-cyclodextrin, which not only enhanced its molecular binding affinity to glutathione (GSH) by a reversible Michael addition, showing 113 times more affinity than that of coumarin itself, but also achieved dynamic real-time sensing of glutathione in living HeLa cells.

Cyclodextrins (CDs), which are cyclic oligosaccharides connected by α-1,4-glycosidic bonds, can be modified by various functional groups on the primary face by the highly reactive C-6 hydroxy groups to synthesize 6-deoxy-CD derivatives.[1–3] Functional groups can cooperate with CDs to recognize multiple organic or biological molecules based on CD encapsulations,[4,5] such as bile acids,[6] biothiols,[7] H_2O_2,[8] ATP,[9] pH,[10] and so on. Therefore, much research has been reported on the synthesis of CD derivatives to enhance the molecular binding affinity and molecular assembly for optical sensing.[11–15]

Recently, Liu and co-workers reported that one dansyl modified β-CD self-assembled to form chiral [1]rotaxane which showed thermally fixed circularly polarized luminescence.[16] Yang and co-workers reported di-pyrene-modified γ-CD self-assembled into nano-strips that could improve electronic circular dichroism and circularly polarized luminescence.[17] The γ-CD could also self-assemble into a metal–organic framework with alkali metal ions,[18] which not only achieved the encapsulation of various dyes for circularly polarized luminescent crystalline materials,[19] but it could also act as a nanoreactor for direct electrocatalyzed ammonia synthesis with hydrogen bonding catalysis.[20] For cell imaging, Pu and co-workers reported a CD-based, renal-clearable and protease-activatable near-infrared fluorescence probe for bioimaging and urinalysis of SARS-CoV-2.[21] However, Ma and co-workers modified various phosphor moieties on β-CD to achieve multicolor photoluminescence.[22] More recently, anthraquinone-modified β-CD enabled a intermolecular inclusion to form a supramolecular polymer, which benefiting from the hydrophobic β-CD cavity was able to shield oxygen molecules, and the anthraquinone group quickly generated 9,10-anthracene diol, which could be used as an emitting ink.[23]

The inclusion modes of CD derivatives, can be divided into intermolecular inclusion and self-inclusion by their host–guest interactions.[24] Due to the presence of a rigid linker or the bridge on the primary surface of CDs, it is easy to form intermolecular inclusions.[24–26] In contrast, if the linker between the CDs and size-matched functional groups was flexible, the CD derivatives were prone to forming a self-inclusion complex,[27,28] or can obtain self-inclusion by a induced-fit mechanism.[29–31] Accompanied by the self-inclusion of functional molecules in the CD cavity, the molecular recognition ability may be enhanced. For example, D-tryptophan-modified β-CD displayed 3.3 times higher binding ability for bile acids than L-tryptophan-modified β-CD because of being deeply self-included.[32]

Herein, we synthesized a coumarin-modified β-cyclodextrin self-inclusion ratiometric fluorescent sensor (**rCP-NN-βCD**) by using flexible ethylenediamine as a linker for dynamic real-time detection of intracellular glutathione GSH (Scheme 1). The self-inclusion configuration of **rCP-NN-βCD** was confirmed from the NMR-ROESY spectrum, which showed that the coumarin moiety was deeply self-included in the β-CD cavity and it was an *E* isomer. When it reacted with GSH by reversible Michael addition, the coumarin was excluded from β-CD cavity, and the reversibility of the inclusion and exclusion states were confirmed by circular dichroism spectrometry. The **rCP-NN-βCD** possessed a high affinity for GSH with a small $K_{d(GSH)}$ at 18.54 μM, a fast Michael addition speed of $t_{1/2}$ = 30 s, and an elimination reaction speed of $t_{1/2}$ = 111 s, which could be applied to the real-time sensing of intracellular GSH.

[a] *College of Chemistry, State Key Laboratory of Elemento-Organic Chemistry, Nankai University, Tianjin 300071, China. E-mail: yuliu@nankai.edu.cn*
[b] *Haihe Laboratory of Sustainable Chemical Transformations, Tianjin 300192, China*
[c] *Faculty of Chemical Engineering, Kunming University of Science and Technology, Kunming 650500, Yunnan, China*

† Electronic supplementary information (ESI) available: Experimental procedures, characterization data, and spectral data. See DOI: https://doi.org/10.1039/d2cc06512f

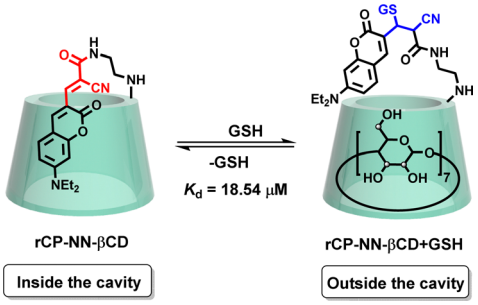

Scheme 1 The self-inclusion of **rCP-NN-βCD** and its reversible Michael addition reaction with GSH.

First, we confirmed the spatial configuration of **rCP-NN-βCD**. As shown in Fig. 1, the obvious correlation in circles 1 and 1′, 2 and 2′ indicated that the coumarin moiety and the covalently β-CD had strong interactions, demonstrating that the coumarin was encapsulated by the β-CD cavity. The correlation of circles 3 and 3′ showed that the hydrogen on the methyl (CH_3)group was closed to the benzene (H_ε and H_δ). In addition, circles 4 and 4′ showed that the H_α and H_β have a strong interaction (Fig. 1 and Fig. S1, ESI†), confirming that the *E* isomer of coumarin was in the β-CD cavity. Subsequently, the ^{1}H-NMR of **rCP-NN-βCD** at different concentrations was performed to distinguish between the self-inclusion and the intermolecular inclusion (Fig. S2, ESI†). With the increase of the concentration of **rCP-NN-βCD** from 0.3 to 10 mM, the chemical shifts of the hydrogen on the coumarin are unchanged, which indicated that the chemical shift does not change with the increase of concentration. This result demonstrated that the encapsulation of coumarin in β-CD cavity was caused by self-inclusion rather than intermolecular inclusion. Therefore, the driving force is mainly from the hydrophobic effects of the β-CD cavity, and the flexible ethylenediamine linker makes it easier for the coumarin to be self-included in the β-CD cavity. Furthermore, the 1D ^{1}H-NMR spectra of **rCP-NN-βCD** and its addition adduct with 2-mercaptoethanol confirmed the progress of the Michael addition reaction (Fig. S3, ESI†).

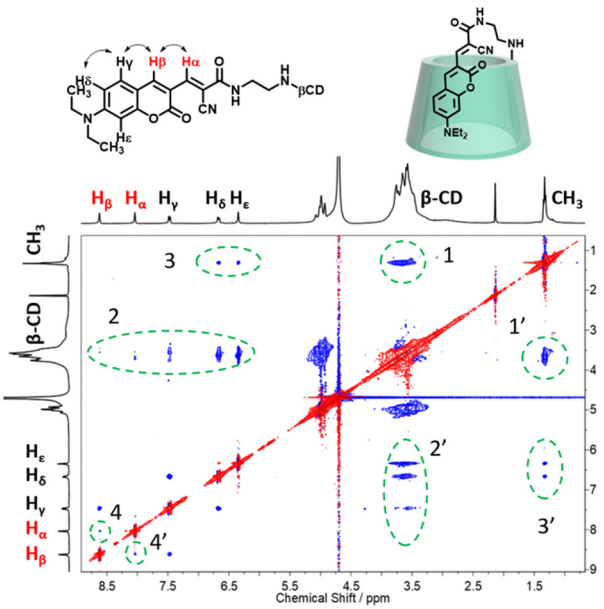

Fig. 1 The NMR-ROESY spectrum of rCP-NN-βCD (4 mM) in D_2O, and the configuration of the coumarin moiety in the β-CD cavity (400 MHz).

Next the UV-Vis absorption and fluorescence spectra were used to evaluate the reversible Michael addition reaction between **rCP-NN-βCD** and GSH in PBS buffer solution.[33,34] With the addition of GSH, the absorption peak at 506 nm decreased rapidly, and was accompanied by a new peak which emerged at 409 nm (Fig. 2a). Meanwhile, the ratiometric fluorescence response was achieved, and the distance between the two maximum fluorescence emission peaks was about 96 nm (Fig. 2b). By fitting the absorption peak ratios (A_{409nm}/A_{506nm}) and the GSH concentrations (Fig. 2c), the associated constant $K_{d(GSH)}$ of **rCP-NN-βCD** was determined to be 18.54 μM. The dose-response curve between **rCP-NN-βCD** and GSH showed that the fluorescence changes were most obvious in the range of 0–0.5 mM, indicating that the **rCP-NN-βCD** possessed a high sensitivity to GSH (Fig. 2d). Based on an S/N ratio of 3, the limit of detection for GSH was determined to be 148 nM (Fig. S4, ESI†). In addition, the fluorescence quantum yields of **rCP-NN-βCD** and **rCP-NN-βCD** + GSH were measured and found to be 3.82% and 12.57%, respectively, (Fig. S5, ESI†).

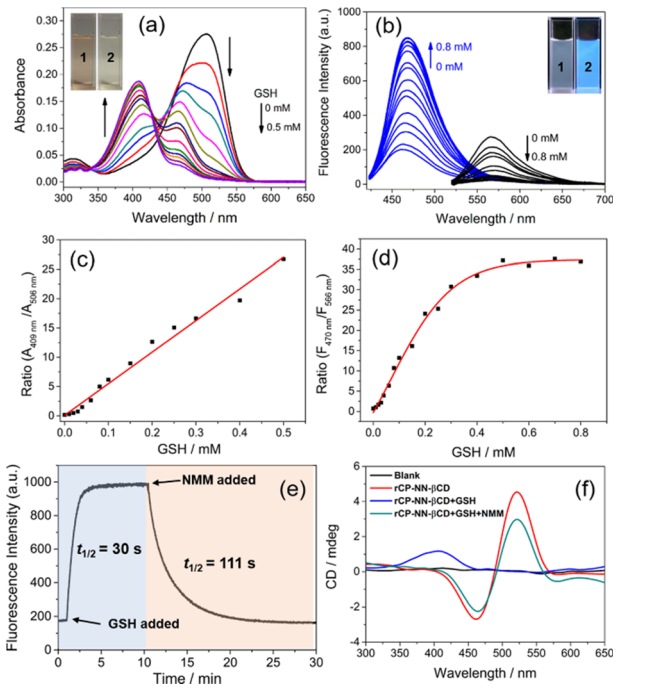

Fig. 2 The UV-Vis absorption (a) and fluorescence spectra (b) of **rCP-NN-βCD** (10 μM) toward GSH (0–0.5 mM) in PBS (Ex = 409 nm, slits: 5/5 nm; Ex = 506 nm, slits: 5/5 nm). Insets: Color and fluorescence of **rCP-NN-βCD** (1) and **rCP-NN-βCD** + GSH (2). The dose–response curves of the UV-Vis absorption (c) and the fluorescence spectra (d) for the reactions of **rCP-NN-βCD** (10 μM) toward GSH (0–0.5 mM). (e) The time-dependent fluorescence emission of **rCP-NN-βCD** at 470 nm by adding GSH (0.5 mM) first, and then followed by NMM (0.5 mM). (f) Circular dichroism spectra of **rCP-NN-βCD** (10 μM) toward GSH (0.5 mM), followed by addition of NMM (0.5 mM).

The UV-Vis absorption spectrum was selected to evaluate the stability and selectivity of **rCP-NN-βCD** to GSH. The **rCP-NN-βCD** showed no obvious structural change at pH 4–10, but displayed an excellent response to GSH at pH 6–10 (Fig. S6, ESI†). Moreover, it displayed better selectivity for GSH than for other intracellular amino acids, some reactive oxygen and nitrogen species (Fig. S7a and c, ESI†). Other intracellular thiols with a lower concentration than GSH, such as cysteine (Cys) and homocysteine (Hcy), can also react with **rCP-NN-βCD** in the same manner. Except for Cys and Hcy, the fluorescence ratio (F_{470nm}/F_{566nm}) and absorption ratio (A_{409nm}/A_{506nm}) of **rCP-NN-βCD** for GSH were enhanced by 70.5 and 95 times, respectively, (Fig. S7b and d, ESI†). Furthermore, we evaluated the detection performance of **rCP-NN-βCD** to GSH in culture medium. The **rCP-NN-βCD** exhibited excellent ratiometric fluorescent responses to GSH (Fig. S8, ESI†), meaning that the **rCP-NN-βCD** could be used in complex intracellular environments. To investigate the reversibility of the reaction between **rCP-NN-βCD** and GSH, *N*-methylmaleimide (NMM) was employed to consume the GSH, and then the $t_{1/2}$ values were calculated. The ^{1}H-NMR experiment was first performed to confirm that there is no interaction between β-CD and NMM (Fig. S9, ESI†), and thereby it had no effect on the reversible Michael addition. With the addition of NMM, the fluorescence emission at 470 nm decreased rapidly, which indicated the recovery of the **rCP-NN-βCD** structure and confirming the reversibility of the reaction (Fig. 2e). The calculation of the reaction time proved that **rCP-NN-βCD** and GSH reacted quickly (forward $t_{1/2}$ = 30 s, reverse $t_{1/2}$ = 111 s) (Fig. S10, ESI†). Meanwhile, the reaction of **rCP-NN-βCD** with Cys or Hcy was also reversible (Fig. S11, ESI†). Although the **rCP-NN-βCD** displayed a good affinity to GSH, the reaction between **rCP-NN-βCD** and GSH was reversible, and the reverse reaction mainly depends on the reduction of the GSH concentration. The addition of NMM reacted with the same concentration of GSH by an irreversible Michael addition, leading to the GSH depletion, thereby greatly promoting the reverse reaction and an almost complete transformation of **rCP-NN-βCD** + GSH to **rCP-NN-βCD**.

In order to investigate the effects of rigid and flexible linkers on the Michael addition reaction, we compared the reaction rates and $K_{d(GSH)}$ between **rCP-NN-βCD** and the reported **rCP-βCD** containing a rigid triazole linker (Scheme S2, ESI†). The **rCP-βCD** displayed a reversible reaction rate toward GSH (forward $t_{1/2}$ = 57.55 s, reverse $t_{1/2}$ = 195.24 s),[7] whereas the response times both in the forward and reverse direction of **rCP-NN-βCD** were faster, and displayed about a 2-fold enhancement. However, a smaller $K_{d(GSH)}$ represented a stronger affinity between the double bond and the mercapto group. The $K_{d(GSH)}$ of **rCP-NN-βCD** was 18.54 μM, which was 6.5 times smaller than with the reported **rCP-βCD** (122 μM), and 113 times smaller than the coumarin without modification of β-CD (**rCP-Al**: 2.809 mM) (Scheme S2, ESI†),[7] indicating that the **rCP-NN-βCD** had a stronger affinity and superior sensitivity to GSH than **rCP-βCD** and coumarin itself. Considering the previous results, **rCP-NN-βCD** has fast reaction kinetics and a high sensitivity to GSH.

Subsequently, we focused on elucidating the rapid reaction rate between **rCP-NN-βCD** and GSH. Circular dichroism spectra of **rCP-NN-βCD** and **rCP-NN-βCD** + GSH were obtained. As shown in Fig. 2f, the spectra of **rCP-NN-βCD** displayed obvious Cotton effects at a concentration of 10 μM. In comparison to the rigid linker probe **rCP-βCD**, no Cotton effects were observed under the same conditions,[7] which suggested that the coumarin moiety on **rCP-NN-βCD** could be self-encapsulated into the β-CD cavity because of the flexible ethanediamine linker. After addition of GSH, the **rCP-NN-βCD** + GSH gave very weak Cotton effects, indicating that the coumarin moiety had escaped from the β-CD cavity but was still around the primary face of β-CD. After that, the addition of NMM caused the elimination reaction, and the Cotton effects were recovered. Meanwhile, the circular dichroism spectra also confirmed that the addition adducts of **rCP-NN-βCD** with Cys or Hcy also escaped from the β-CD cavity (Fig. S12, ESI†). Therefore, it was deduced that **rCP-NN-βCD** formed a self-inclusion molecular complex, and that subsequently the coumarin moiety escaped from the cavity as a result of the excellent water solubility of the coumarin addition product, and then the self-inclusion configuration was recovered during the elimination reaction. Structurally, the coumarin moiety could be encapsulated into the cavity to form self-inclusion due to the existence of a flexible linker, and the double bond of coumarin near the primary surface of β-CD was more favorable for realization of the Michael addition reaction, accompanied by faster reaction kinetics with the assistance of numerous hydroxyl groups on β-CD.[35]

For real-time sensing of intracellular GSH, we carried out time dependent imaging in living HeLa cells. The cells were first incubated with **rCP-NN-βCD** for 6 h to observe the internalization of the **rCP-NN-βCD** (Fig. S13, ESI†). The **rCP-NN-βCD** emitted bright fluorescence in both the blue and green channels, confirming that **rCP-NN-βCD** could be internalized and reacted with GSH. Subsequently, the NMM was selected to disrupt the intracellular redox homeostasis. Real-time ratiometric imaging showed that the green/blue ratio increased (within 120 s) and then reached an equilibrium after the addition of NMM (Fig. 3 and Fig. S14, ESI†). The GSH concentration variation was observed from representative green/blue ratio images (Fig. 3a–d). The fluorescence intensity quantitative analysis of the green/blue ratio also showed the enhancement change (Fig. 3e). In contrast, the green/blue ratio did not change when incubated with NMM-free culture medium for 440 s (Fig. S15 and S16, ESI†). This result indicated that the **rCP-NN-βCD** could be used for real-time sensing of intramolecular GSH.

In summary, we synthesized a β-CD-based self-inclusion probe, **rCP-NN-βCD**, for enhanced dynamic monitoring of intracellular GSH. It had a strong molecular binding affinity for GSH with a small $K_{d(GSH)}$ at a concentration of 18.54 μM, showing 113 times more affinity for GSH than that of coumarin itself. The coumarin moiety can be deeply self-encapsulated into the β-CD cavity and the addition product with GSH was excluded from the β-CD cavity. The **rCP-NN-βCD** was successfully used for real-time detection of GSH in HeLa cells, providing a new approach for the development of optical sensors.

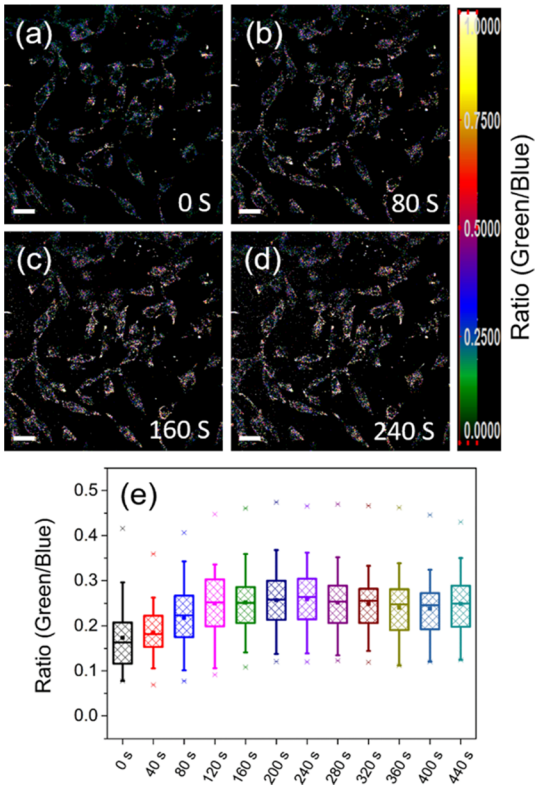

Fig. 3 (a–d) Representative ratiometric images (green/blue) displaying real-time changes of GSH in HeLa cells treated with NMM (5 mM) (scale bar: 30 μm). (e) The fluorescence intensity quantitative analysis of GSH dynamic changes in individual HeLa cells (n = 30).

We gratefully acknowledge financial support received from the following: the National Natural Science Foundation of China (Grant No. 22131008, 21807038, 52263011, 51963012), the China Postdoctoral Science Foundation (Grant No. 2021T140343), and the Haihe Laboratory of Sustainable Chemical Transformations.

Conflicts of interest

There are no conflicts to declare.

Notes and references

1 Z. Liu and Y. Liu, *Chem. Soc. Rev.*, 2022, **51**, 4786–4827.
2 J. Liu, B. Wang, C. Przybylski, O. Bistri-Aslanoff, M. Ménand, Y. Zhang and M. Sollogoub, *Angew. Chem., Int. Ed.*, 2021, **60**, 12090–12096.
3 F. Bellia, D. La Mendola, C. Pedone, E. Rizzarelli, M. Saviano and G. Vecchio, *Chem. Soc. Rev.*, 2009, **38**, 2756–2781.
4 T. L. Mako, J. M. Racicot and M. Levine, *Chem. Rev.*, 2019, **119**, 322–477.
5 B. Zhao, L. Jiang and Q. Jia, *Chin. Chem. Lett.*, 2022, **33**, 11–21.
6 Y. M. Zhang, X. Xu, Q. Yu, Y. H. Liu, Y. H. Zhang, L. X. Chen and Y. Liu, *J. Med. Chem.*, 2017, **60**, 3266–3274.
7 Z. Liu, W. Zhou, J. Li, H. Zhang, X. Dai, Y. Liu and Y. Liu, *Chem. Sci.*, 2020, **11**, 4791–4800.
8 X. Wei, R. Dong, D. Wang, T. Zhao, Y. Gao, P. Duffy, X. Zhu and W. Wang, *Chem. – Eur. J.*, 2015, **21**, 11427–11434.
9 W. Zhang, P. Xiao, L. Lin, F. Guo, Q. Wang, Y. Piao and G. Diao, *Chin. Chem. Lett.*, 2022, **33**, 4043–4047.
10 Y. M. Zhang, M. Han, H. Z. Chen, Y. Zhang and Y. Liu, *Org. Lett.*, 2013, **15**, 124–127.
11 W. F. Lai, A. L. Rogach and W. T. Wong, *Chem. Soc. Rev.*, 2017, **46**, 6379–6419.
12 Z. Liu, W. Lin and Y. Liu, *Acc. Chem. Res.*, 2022, **55**, 3417–3429.
13 S. Gnaim, A. Scomparin, A. Eldar-Boock, C. R. Bauer, R. Satchi-Fainaro and D. Shabat, *Chem. Sci.*, 2019, **10**, 2945–2955.
14 Y. Sugita, D. Aoki, M. Tokita and H. Otsuka, *Chem. Commun.*, 2022, **58**, 3067–3070.
15 D. Larsen, M. Ferreira, S. Tilloy, E. Monflier and S. R. Beeren, *Chem. Commun.*, 2022, **58**, 2287–2290.
16 X. Song, X. Zhu, S. Qiu, W. Tian and M. Liu, *Angew. Chem., Int. Ed.*, 2022, **61**, e202208574.
17 C. Tu, W. Wu, W. Liang, D. Zhang, W. Xu, S. Wan, W. Lu and C. Yang, *Angew. Chem., Int. Ed.*, 2022, **61**, e202203541.
18 I. Roy and J. F. Stoddart, *Acc. Chem. Res.*, 2021, **54**, 1440–1453.
19 L. Hu, K. Li, W. Shang, X. Zhu and M. Liu, *Angew. Chem., Int. Ed.*, 2020, **59**, 4953–4958.
20 X. Dai, L. Tian, Z. Liu, W. Xu, Y. P. Liu and Y. Liu, *ACS Nano*, 2022, **16**, 18398–18407.
21 S. S. Liew, Z. Zeng, P. Cheng, S. He, C. Zhang and K. Pu, *J. Am. Chem. Soc.*, 2021, **143**, 18827–18831.
22 D. Li, F. Lu, J. Wang, W. Hu, X. M. Cao, X. Ma and H. Tian, *J. Am. Chem. Soc.*, 2018, **140**, 1916–1923.
23 L. Chen, Y. Chen, H. G. Fu and Y. Liu, *Adv. Sci.*, 2020, **7**, 2000803.
24 P. Evenou, J. Rossignol, G. Pembouong, A. Gothland, D. Colesnic, R. Barbeyron, S. Rudiuk, A. G. Marcelin, M. Menand, D. Baigl, V. Calvez, L. Bouteiller and M. Sollogoub, *Angew. Chem., Int. Ed.*, 2018, **57**, 7753–7758.
25 G. Yu, X. Zhao, J. Zhou, Z. Mao, X. Huang, Z. Wang, B. Hua, Y. Liu, F. Zhang, Z. He, O. Jacobson, C. Gao, W. Wang, C. Yu, X. Zhu, F. Huang and X. Chen, *J. Am. Chem. Soc.*, 2018, **140**, 8005–8019.
26 Z. Liu, X. Dai, Q. Xu, X. Sun and Y. Liu, *Chin. J. Chem.*, 2022, **40**, 493–499.
27 J. W. Park, S. Y. Lee, H. J. Song and K. K. Park, *J. Org. Chem.*, 2005, **70**, 9505–9513.
28 H. F. Nelissen, M. C. Feiters and R. J. Nolte, *J. Org. Chem.*, 2002, **67**, 5901–5906.
29 H. Zhang, B. Zhang, M. Zhu, S. M. Grayson, R. Schmehl and J. Jayawickramarajah, *Chem. Commun.*, 2014, **50**, 4853–4855.
30 Y. Liu, C. F. Ke, H. Y. Zhang, J. Cui and F. Ding, *J. Am. Chem. Soc.*, 2008, **130**, 600–605.
31 R. Nishiyabu and K. Kano, *Eur. J. Org. Chem.*, 2004, 4985–4988.
32 H. Wang, R. Cao, C. F. Ke, Y. Liu, T. Wada and Y. Inoue, *J. Org. Chem.*, 2005, **70**, 8703–8711.
33 J. Chen, X. Jiang, S. Carroll, J. Huang and J. Wang, *Org. Lett.*, 2015, **17**, 5978–5981.
34 Z. Liu, X. Zhou, Y. Miao, Y. Hu, N. Kwon, X. Wu and J. Yoon, *Angew. Chem., Int. Ed.*, 2017, **56**, 5812–5816.
35 K. Takahashi, *Chem. Rev.*, 1998, **98**, 2013–2034.